Comput Geosci (2017) 21:909–919
DOI 10.1007/s10596-017-9658-8

ORIGINAL PAPER

# Comparison of linear reconstructions for second-order finite volume schemes on polyhedral grids

**Robert Klöfkorn**[1] · **Anna Kvashchuk**[2] · **Martin Nolte**[3]

Received: 17 October 2016 / Accepted: 28 April 2017 / Published online: 20 May 2017


**Abstract** Improved and enhanced oil recovery methods require sophisticated simulation tools to predict the injected flow pass together with the chemical reactions inside it. One approach is application of higher-order numerical schemes to avoid excessive numerical diffusion that is very typical for transport processes. In this work, we provide a first step towards higher-order schemes applicable on general polyhedral and corner-point grids typically used in reservoir simulation. We compare three possible approaches of linear reconstruction and slope limiting techniques on a variety of different meshes in two and three spatial dimensions and discuss advantages and disadvantages.

**Keywords** Second-order finite volume · Linear reconstruction · Polyhedral grids · DUNE · OPM

✉ Robert Klöfkorn
robert.kloefkorn@iris.no

Anna Kvashchuk
a.kvashchuk@stud.uis.no

Martin Nolte
nolte@mathematik.uni-freiburg.de

[1] International Research Institute of Stavanger, Thormøhlensgt. 55, 5008 Bergen, Norway

[2] University of Stavanger, P.O. Box 8600 Forus, 4036 Stavanger, Norway

[3] University of Freiburg, Hermann-Herder-Str. 10, 79104 Freiburg, Germany

## 1 Introduction

In a typical oil reservoir, more than half of the oil remains trapped in the reservoir after abandonment. That is why government agencies and companies are interested in improved (enhanced) oil recovery (IOR and EOR) methods that can increase oil production significantly. The injection of gas, ”smart water,” polymers, etc. in the reservoir is promising technique in the family of IOR methods. In order to implement these techniques successfully, companies need a simulator that can predict the injected flow pass together with the chemical reactions inside it. Presence of chemical reactions in the flow makes numerical approximations and modeling a challenging task. The typically used low-order methods suffer from excessive numerical diffusion that leads to smeared fronts and incorrect species concentrations (cf. [19] and references therein).

One suitable way to reduce the numerical diffusion in transport phenomena modeling is provided by higher-order numerical methods. Over the last decades, a lot of different types of higher-order numerical methods were developed and studied, e.g., finite volume, finite element, and discontinuous Galerkin schemes (cf. [28] and references therein). These methods are widely used not only in subsurface application [1, 13, 27] but also in global climate modeling [17], or computational fluid dynamics applications [18].

In reservoir simulation, traditionally, finite volume methods are favored over finite element methods due to conservation properties, simplicity, and robustness on general *polyhedral* meshes, which are of great help in resolving complicated geological structures. Higher-order approaches for finite volume schemes originate with early works from the 1970s conducted by [23], which gained further

developed in many works, e.g., [5, 6, 15, 16, 22]. However, such techniques are not available in standard reservoir simulators to the extent necessary for IOR and EOR methods.

In this paper, we discuss three (dimension-independent) approaches to implement second-order finite volume schemes for tracer transport on general polyhedral meshes. These approaches are compared on a series of different meshes in two and three space dimensions. The implementation is based on the DUNE framework [2, 3, 9] and is available under an open-source license.

## 2 Problem formulation

Finite volume schemes were developed for first-order hyperbolic conservation laws of the form

$$\partial_t u + \nabla \cdot f(x,t,u) = 0, \tag{1}$$

in some domain $\Omega \subset \mathbb{R}^d$, subject to initial values and suitable boundary conditions.

Let $\mathcal{T}$ be a computational grid of the domain $\Omega \subset \mathbb{R}^d$ and denote by $\partial\mathcal{T}$ a tessellation of the boundary $\partial\Omega$. Following the DUNE concept, we consider intersections of an element $E \in \mathcal{T}$ either with an adjacent element or with the domain boundary:

$$\mathcal{I}(E) := \big\{(E,F) \;\big|\; F \in \mathcal{T} \cup \partial\mathcal{T}, \dim E \cap F = d-1\big\}.$$

For each intersection $i = (E,F)$, we denote by $\nu_i$ the unique outer normal to $E$ on $E \cap F$. By abuse of notation, we will also use the symbol $i$ to denote $E \cap F$. By $\mathcal{I}(\mathcal{T}) := \bigcup_{E\in\mathcal{T}} \mathcal{I}(E)$, we denote the set of all intersections.

Let us assume that we are given cell averages $(u_E^0)_{E\in\mathcal{T}}$ for the initial data. Then, a classical first-order finite volume scheme for Eq. 1 reads as follows:

$$u_E^{n+1} = u_E^n - \frac{\Delta t}{|E|} \sum_{i\in\mathcal{I}(E)} g_i\big(t^n, u_{i,-}^n, u_{i,+}^n\big). \tag{2}$$

Here, the numerical flux $g_i$ is an approximation of the flux through intersection $i$ at a given time, i.e.,

$$g_i(t, u_{i,-}, u_{i,+}) \approx \int_i f(x,t,u)\cdot\nu_i \, dx,$$

which we require to be consistent, conservative, and monotone. For the definition of these terms, we refer to standard text books on finite volume schemes, such as [21] which also describes the Enquist-Osher flux used for numerical computations carried out in this paper.

The values $u_{i,\pm}^n$ are defined as follows:

$$u_{i,-}^n = u_E^n \quad \text{and} \quad u_{i,+}^n = \begin{cases} u_{E'}^n & i = (E,E') \in \mathcal{I}(\mathcal{T}), \\ b_i^n(u_E^n) & i = (E,\partial\Omega) \in \mathcal{I}(\mathcal{T}), \end{cases}$$

where we require a mapping $b_i^n : \mathcal{U} \to \mathcal{U}$ for each boundary intersection $i = (E,F) \in \mathcal{I}(\mathcal{T})$, $F \in \partial\mathcal{T}$, and each time $t^n$.

We seek to compute the function $u : \mathbb{R}^d \to \mathcal{U} \subset \mathbb{R}^r$, where $\mathcal{U}$ is the set of states and $r$ is the dimension of the range space. Without loss of generality, we assume $r = 1$ but all results and implementations hold for $r > 1$.

## 3 Second-order finite volume schemes

For the considered conservation law, a variety of higher-order schemes is available and has been studied intensively throughout the past two decades. In this paper, we consider slope limiting techniques applied to linear reconstructions introduced in early works such as [23] and also found in standard textbooks such as [12, 21, 24, 29]. In particular, we compare three different approaches for reconstruction of linear functions on arbitrary polyhedral meshes.

For a higher-order finite volume scheme based on reconstructions, we want to compute a linear reconstruction for each element $L_E$, which, in its turn, is then used to compute the numerical fluxes in Eq. 2,

$$u_E^{n+1} = u_E^n - \frac{\Delta t}{|E|} \sum_{i\in\mathcal{I}(E)} g_i\big(t^n, L_{i,-}^n, L_{i,+}^n\big), \tag{3}$$

where $L_{i,-}^n$ and $L_{i,+}^n$ are the evaluations of the linear reconstructions on the intersections barycenter on element $E$ and its neighbor $E_i$, respectively. As described in [8], the linear functions are defined as follows:

$$L_E(\mathbf{x}) = u_E + \nabla L_E \cdot (\mathbf{x} - \mathbf{w}_E), \tag{4}$$

where $\mathbf{w}_E$ is the barycenter of $E$ and $\nabla L_E \in \mathbb{R}^{r\times d}$ is the gradient of $L_E$ that needs to be computed. The computation of $\nabla L_E$ only relies on the cell and its neighbor barycenter, the volume, intersection normals at the center of the intersection, and the solution $u$ on the element and its surrounding neighbors. In the following, we compare three different techniques to compute a suitable reconstruction of the linear function $L_E$.

### 3.1 Least squares reconstruction

A simple and straightforward approach to obtain a linear reconstruction is to compute a least squares approximation (see, e.g., [12]). More precisely, we seek a reconstruction $L_E$ satisfying (4) and

$$L_E(\mathbf{w}_{E'}) = u_{E'} \quad \forall (E,E') \in \mathcal{I}(E). \tag{5}$$

As this system is overdetermined even on simplex grid, we only require condition (5) to be fulfilled in a least squares sense. Let us assume that the neighbors $\{E' | (E,E') \in \mathcal{I}(E)\}$ are enumerated as $\{E_1, \dots, E_{N_E}\}$ with $N_E$ being the number of neighbors of cell $E$. Then, the solution to

the above problem can be readily computed by solving the linear $d \times d$ system

$$\begin{aligned}(\mathbf{A}_E^T \mathbf{A}_E)\, \nabla L_E &= \mathbf{A}_E^T \mathbf{b}_E,\\ \mathbf{A}_E &:= (\mathbf{w}_{E_l} - \mathbf{w}_E)_{l=1,\dots,N_E} \in \mathbb{R}^{N_E \times d},\\ \mathbf{b}_E &:= (u_{E_l} - u_E)_{l=1,\dots,N_E} \in \mathbb{R}^{N_E}.\end{aligned}$$

To avoid oscillations, we apply a limiter function to the reconstruction (4), i.e., for $l = 1, \dots, N_E$ we compute

$$m_l := \begin{cases} 0 & \text{if } g_l\, d_l \le 0,\\ d_l/g_l & \text{if } g_l\, d_l > 0 \text{ and } |g_l| > |d_l|,\\ 1 & \text{otherwise.}\end{cases} \tag{6}$$

where

$$g_l = \nabla L_E \cdot (\mathbf{w}_{E_l} - \mathbf{w}_E) \quad \text{and} \quad d_l := u_{E_l} - u_E.$$

Notice that $g = \mathbf{A}_E \nabla L_E$ and $d = \mathbf{b}_E$ in our case. The limited reconstruction is then obtained by

$$\tilde{L}_E(\mathbf{x}) = u_E + \min_{l=1,\dots,N_E} m_l\, \nabla L_E \cdot (\mathbf{x} - \mathbf{w}_E). \tag{7}$$

The function in Eq. 6 is often referred to as *Minmod* limiter. Other limiter functions such as *van Leer* or *Superbee* can be applied seamlessly. A comprehensive list of limiter functions is provided in standard textbooks such as [12, 21, 24, 29].

### 3.2 Selective linear reconstruction

Another approach to compute linear reconstructions was introduced in [10] and improved in [30] to work with conforming triangular meshes. In [8], this approach was generalized to work with non-conforming meshes in two and three space dimensions.

A set of possible linear reconstruction can be obtained by using the cell's value and $d$ (the spatial dimension) disjoint neighboring cell values, where each linear reconstruction has to fulfill the conditions in Eq. 5. Let $j$ denote the set of $d$ neighboring elements which have been selected to compute $L_j$. Figure 1b shows an example where neighbors 1 and 2 have been used to compute $L_j$ with $j := \{1, 2\}$. The set of all possible combinations is denoted by $Y_E$ and contains $\frac{N_E!}{d!(N_E-d)!}$ combinations, where $N_E$ is the number of neighbors. For all $j \in Y_E$, we need to solve a $d \times d$ linear system of the form

$$\begin{aligned}\nabla L_j &= \mathbf{A}_j^{-1}\, \mathbf{b}_j,\\ \mathbf{A}_{j_l} &:= (\mathbf{w}_{E_{j_l}} - \mathbf{w}_E),\ \forall l = 1, ..., d,\\ \mathbf{b}_{j_l} &:= u_{E_{j_l}} - u_E,\ \forall l = 1, ..., d.\end{aligned}$$

Since the size of $\mathbf{A}_{j_l}$ does only depend on the spatial dimension $d$, the inverse can be easily computed using Cramer's rule even if we consider systems of equations. As described in [8], special treatment is necessary in case the rows of $\mathbf{A}_{j_l}$ are linearly dependent, which, for example, occurs on

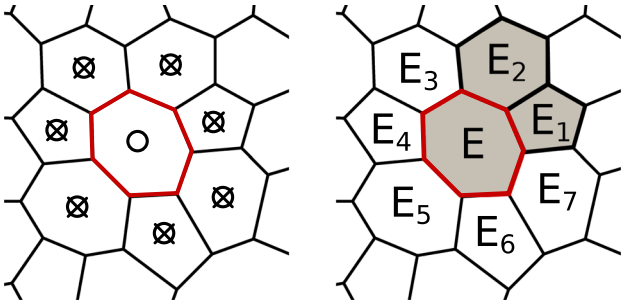


(a) Least squares reconstruction (b) Selective reconstruction

**Fig. 1** Stencils for two of the considered reconstruction methods. In the least squares approach (**a**), all neighbors are considered for reconstruction and limiting, whereas in the selective approach (**b**), all pairs of $d$ disjoint neighbors are considered

Cartesian grids. For polygonal and polyhedral grids in particular, another problem arises. When an element has many neighbors, the number of linear functions to compute grows super linear as described earlier. In the example from Fig. 1, one gets 21 possible linear functions to compute. This number is even bigger in our 3D examples where cells with 8 neighbors and thus 56 combinations occur.

In comparison to the above-presented least squares approach in order to apply limiter function, we now consider only a subset of all neighbors, e.g., the function values at neighboring cells $\tilde{j} := \{3, 4, 5, 6, 7\}$. For each linear reconstruction $j \in Y_E$, we apply a limiter using the cell values of cells contained in $\tilde{j}$. For each cell $i \in \tilde{j}$, we compute

$$g_{j,i} := \nabla L_j \cdot (\mathbf{w}_{E_i} - \mathbf{w}_E) \quad \text{and} \quad d_{j,i} := u_{E_i} - u_E,$$

$$m_{j,i} := \begin{cases} 0 & \text{if } g_{j,i}\, d_i < 0,\\ d_i/g_{j,i} & \text{if } g_{j,i}\, d_i > 0 \text{ and } |g_{j,i}| > |d_i|,\\ 1 & \text{otherwise.}\end{cases} \tag{8}$$

which then yields a limited reconstruction $\widetilde{L}_j$ by selecting the minimal value of all $m_{j,i}$,

$$\widetilde{L}_j(\mathbf{x}) := u_E + \min_{i \in \tilde{j}} m_{j,i} \nabla L_j \cdot (\mathbf{x} - \mathbf{w}_E).$$

From the set of admissible linear reconstructions $\widetilde{L}_j$, $j \in Y_E$, we select the one with the steepest gradient.

### 3.3 Optimization-based reconstruction

A more recent approach by May and Berger [7, 26] considers reconstruction and limitation as a single step. Their goal is a reconstruction $L_E$ satisfying (4) and approximating condition (5) on the neighboring values in an $l^1$-optimal sense, i.e., $L_E$ minimizes

$$J(L) := \sum_{i=1}^{N_E} \left| u_{E_i} - L(\mathbf{w}_{E_i}) \right|.$$

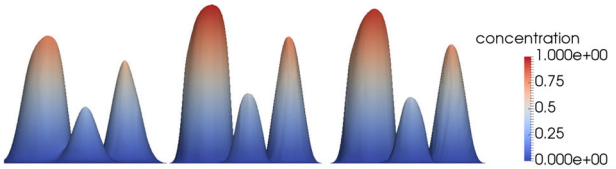


(a) Y-Z Plane

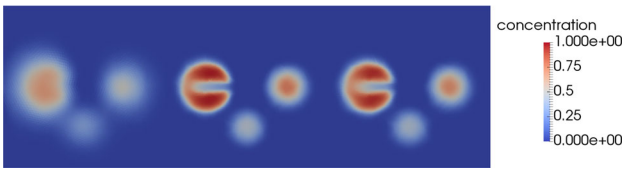


(b)(left) 1st order, (middle) 2nd order selected reconstruction, and (right) 2nd order least squares.

**Fig. 2** Results for the solid body rotation problem at $T_{\text{final}} = 1.5708$

To avoid oscillations, we additionally enforce the monotonicity condition

$$\min\{u_E, u_{E_i}\} \leq L_E(w_{E_i}) \leq \max\{u_E, u_{E_i}\}. \tag{9}$$

for $i = 1, \ldots, N_E$. It can be shown that the gradient $\nabla L_E$ of the reconstruction $L_E$ minimizing $J(L)$ subject to Eqs. 4 and 9 is given as the solution of the following linear programming problem:

$$\begin{aligned} &\text{maximize} && \sum_{l=1}^{N_E} \operatorname{sign}(d_l)\,(\mathbf{w}_{E_l} - \mathbf{w}_E)\cdot\nabla L_E, \\ &\text{subject to} && 0 \leq \operatorname{sign}(d_l)\,(\mathbf{w}_{E_l} - \mathbf{w}_E)\cdot\nabla L_E \leq |d_l|. \end{aligned}$$

This problem can be solved by a variant of the classical simplex algorithm detailed in the appendix of [26]. Our initial guess is $\nabla L_E = 0$, as the constant reconstruction must be admissible. Moreover, we need to select $d$ initially active constraints from the set

$$0 \leq \operatorname{sign}(d_l)\,(\mathbf{w}_{E_l} - \mathbf{w}_E)\cdot\nabla L_E \quad l = 1, \ldots, N_E.$$

Notice that for the method to work reliably, care must be taken to choose $d$ constraints with linear independent $\mathbf{w}_{E_l} - \mathbf{w}_E$. While usually it is not an issue on fully unstructured grids, it naturally arises for Cartesian or extruded grids.

## 4 Modifications for implicit time stepping

Both reconstructions work fine with implicit Runge-Kutta methods based on Jacobian-free Newton-Krylov methods, which are, for example, described in [20]. The following modifications to the procedures above have to be applied. For both schemes, the limiter functions is only to be computed once per Runge-Kutta step and all applications of the operator during Newton and Krylov solves have to use the same $m$ to scale the gradient of the linear reconstruction on one element. For the selective reconstruction scheme, the selected combination of neighboring elements to compute the linear reconstruction is also fixed during Newton and Krylov solves.

## 5 Implementation

The implementation of the finite volume scheme and the reconstruction is based on the DUNE framework (cf. [2, 3]). This work uses the DUNE release 2.4 [4]. The finite volume scheme and the reconstructions are openly available

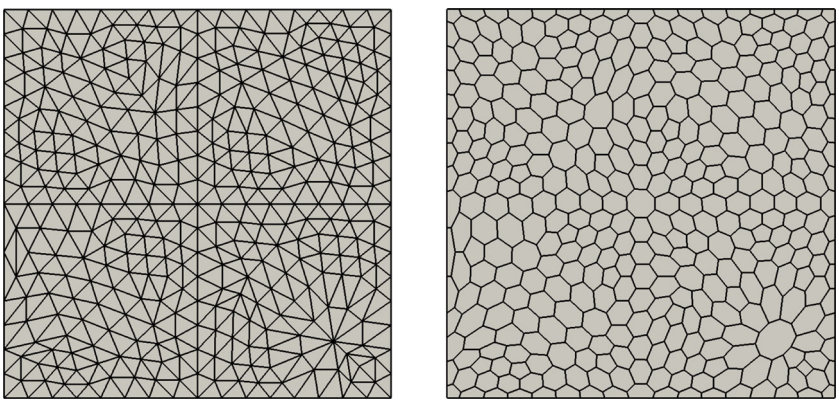

(a) Triangles (b) Polygons

**Fig. 3** Grids used for the 2D test cases. The *triangular grid* series is part of *Benchmark on Discretization Schemes for Anisotropic Diffusion Problems on General Grids* [14]. The *polygonal grid* is the dual grid of the triangular grid constructed by connecting the cell barycenters with the edge midpoints

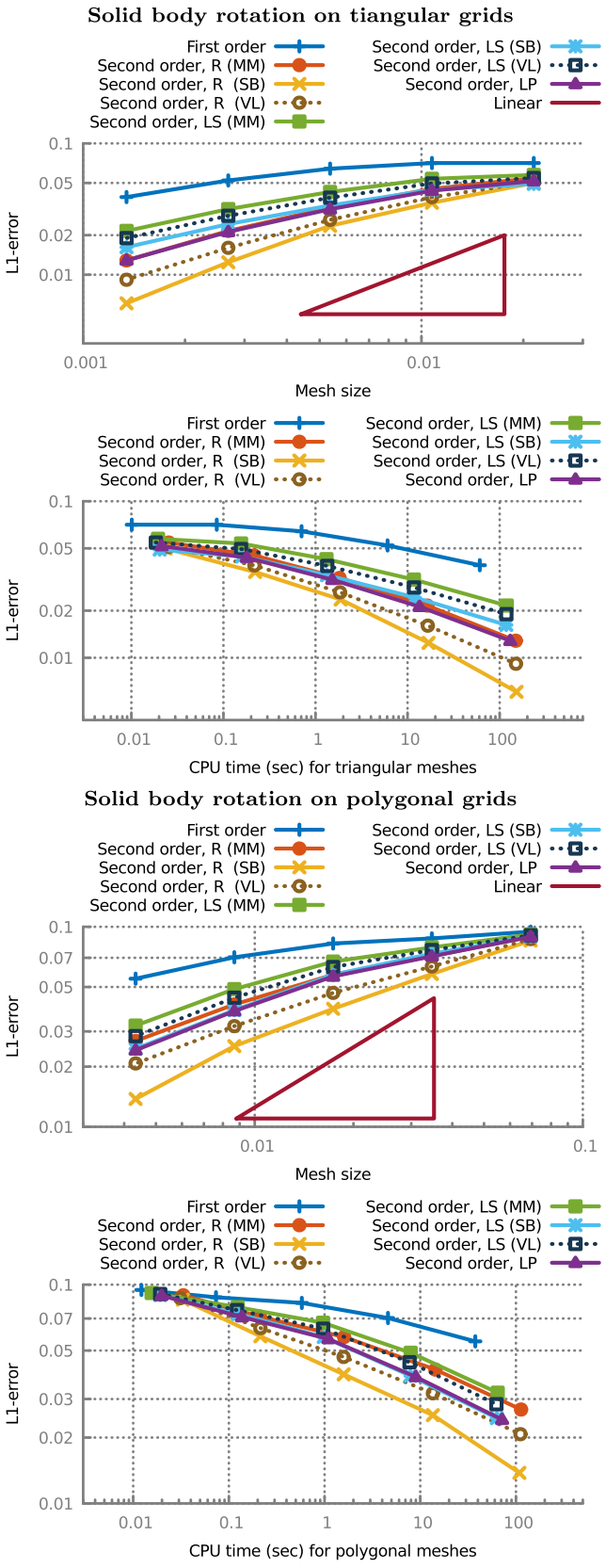


**Fig. 4** Convergence and CPU times for the solid body rotation test case on a series of triangular (*top*) and polygonal (*bottom*) grids at $T_{\text{final}} = 1.5708$

in the DUNE module `polygonal-fv`.[1] Furthermore, the code also uses the discretization module DUNE-FEM [9]. The `PolygonGrid`.[2] used for the 2D computations is a standalone implementation. The `PolyhedralGrid` used for the 3D computations is part of the Open Porous Media (OPM) Initiative.[3]

## 6 Numerical simulation results and convergence study

In the following, we compare presented approaches to reconstruction on a variety of meshes in two and three spatial dimensions. For selected meshes, we will also compare different limiter functions. Finally, we show that the presented approaches work on grids that are typically used in reservoir simulation.

### 6.1 Solid body rotation in 2D

As a first test, we consider a standard benchmark for higher-order finite volume schemes, the so-called solid body rotation, see, e.g., [25]. In this test case, three different shapes are rotating at a constant velocity around the center of the unit square $[0, 1]^2 \subset \mathbb{R}^2$.

More precisely, we consider a transport problem, i.e., $f(x, u) = u\, v(x)$, where the velocity field is given by $v(x) = (\frac{1}{2} - x_2, x_1 - \frac{1}{2})$. For the initial data, we consider a slotted cylinder at $c_1 = (\frac{1}{2}, \frac{3}{4})^T$, a cone at $c_2 = (\frac{1}{2}, \frac{1}{4})^T$, and a hump at $c_3 = (\frac{1}{4}, \frac{1}{2})^T$, each with a radius of $r = \frac{1}{15}$, i.e.,

$$u_0(x) = \begin{cases} 1, & |x - c_1| < r \text{ and} \\ & \left(|x_1 - c_{1,1}| \geq \frac{1}{40} \text{ or } x_2 \geq c_{1,2} + \frac{1}{10}\right), \\ 1 - \frac{1}{r}\,|x - c_2| & |x - c_2| < r, \\ \frac{1}{4} + \frac{1}{4}\,\cos\left(\frac{\pi}{r}\,|x - c_3|\right), & |x - c_3| < r, \\ 0, & \text{otherwise.} \end{cases}$$

All boundary values are assumed to be zero.

We compute the solution of the solid body rotation for a quarter rotation until $T_{\text{final}} = 1.5708$. The results for first (1st) and second (2nd) order schemes are shown in Fig. 2. Typical grids used for the selection of 2D test cases are shown in Fig. 3.

In Fig. 4 (top), we present the results for variety of different schemes on a series of triangular meshes. All second-order schemes work well, the selected reconstruction

[1] https://gitlab.dune-project.org/robert.kloefkorn/polygonal-fv.git.

[2] https://gitlab.dune-project.org/martin.nolte/dune-polygongrid.

[3] http://www.opm-project.org. patched version at https://github.com/dr-robertk

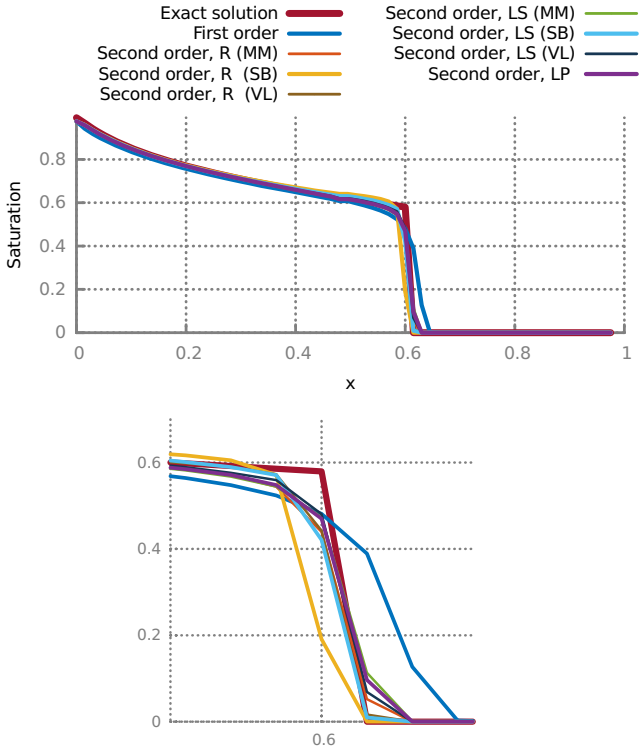


**Fig. 5** Solutions of the Buckley-Leverett problem on a polygonal grid. The *plot* shows the solution for a fixed $y$-coordinate, $y = 0.5$. The first-order scheme and the selected reconstruction with Superbee limiter deviate significantly from the shock position

being the best in terms of accuracy and accuracy vs. run time. The least squares approach (LS) provides the weakest second-order scheme followed by the optimization scheme (LP) which in this case produces results very similar to the selected reconstruction (R) using a Minmod limiter function. The best approaches is provided using the R scheme and either a Superbee or van Leer limiter. It is very clear that all second-order approaches outperform the first-order scheme by orders of magnitude in terms of accuracy vs. run time. A similar behavior is discovered for the schemes when run on the series of polygonal meshes in Fig. 4 (bottom). In contrast to the triangular meshes, the LS scheme with Superbee limiter performs better than the R scheme with Minmod. Overall, the R scheme with Van Leer or Superbee and the optimization scheme (LP) are the best choices in both cases.

### 6.2 Buckley-Leverett problem in 2D

In this section, we test the proposed schemes for non-linear scalar problem. More precisely, we consider a Buckley-Leverett type problem, i.e., $f(x,u) = f_{BL}(u)\, v(x)$, where

$$f_{BL}(u) = \begin{cases} 1 & \text{if } u > 1, \\ 0 & \text{if } u < 0, \\ u^2/(u^2 + \frac{1}{2}(1-u)^2) & \text{otherwise.} \end{cases}$$

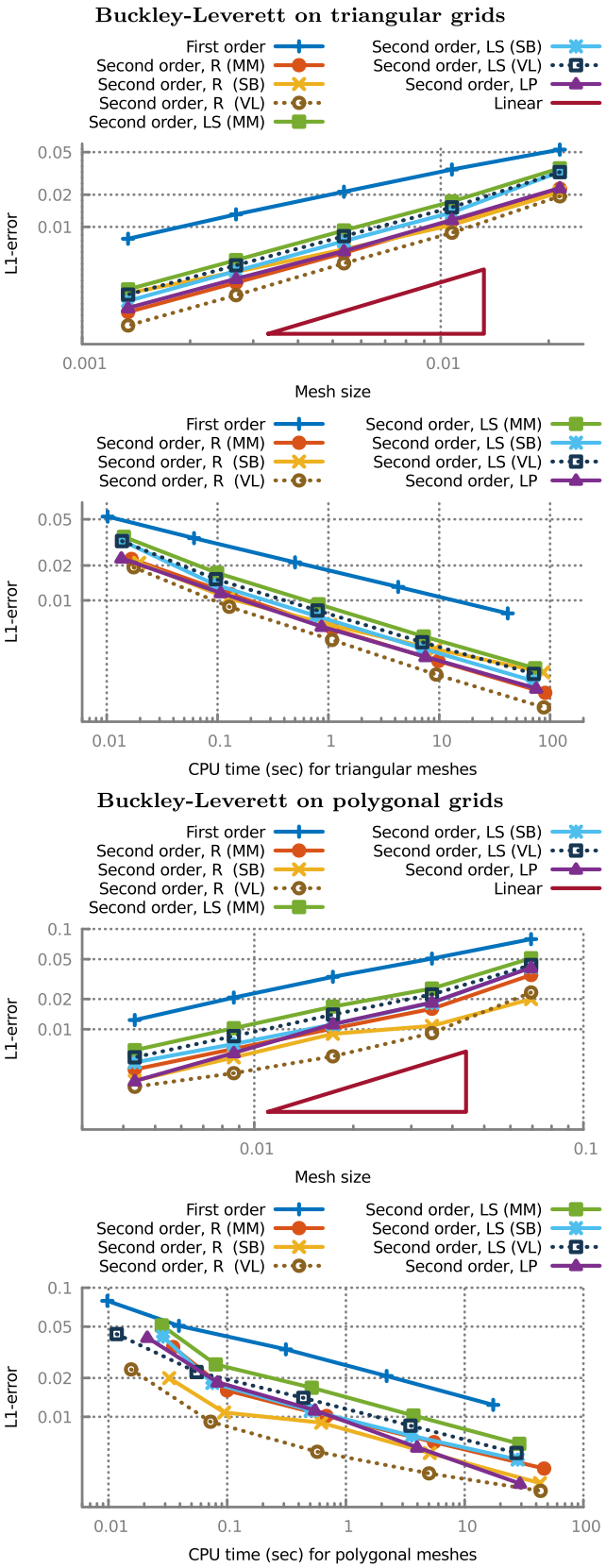


**Fig. 6** Convergence and CPU times for the Buckley-Leverett test case on a series of triangular (*top*) and polygonal (*bottom*) grids at $T_{\text{final}} = 0.45$

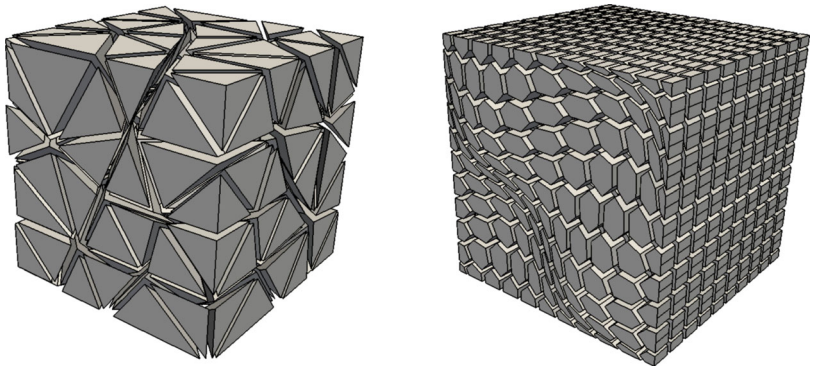

(a) Tetrahedra (b) Prisms with hexagonal bases

**Fig. 7** Grids used for the 3D test cases. Both grid series are part of the 3D Benchmark on Discretization Schemes for Anisotropic Diffusion Problems on General Grids [11]

and the velocity is simply $v(x) = (1, 0)^T$. This is a simplified model for water-oil displacement in a reservoir. Again, we consider the domain $[0, 1]^2 \subset \mathbb{R}^2$.

Initially, the shock is located at $x = 0$. The shock, which travels to the right, is followed by a rarefaction wave. For this problem, a quasi-exact solution can be computed (see for example [24, Chapter 4.7], which allows us to study the convergence behavior of the schemes). We also use the quasi-exact solution to set the boundary values for all schemes.

In Fig. 5, the plot of the solution along a line with fixed $y$-coordinate $y = 0.5$ is presented. Due to the non-linearity of the problem, a self-sharpening effect of the front is present. However, the first-order scheme does not correctly predict the position of the front. This is cured by most of the second-order schemes, except for the selected reconstruction with the Superbee limiter, which seems to lag a bit behind.

In Fig. 6, a comparison of the different schemes in terms of accuracy is presented. Again, the second-order schemes outperform the first-order scheme in terms of accuracy and in terms of run time to accuracy. Similar to the linear test case, the selected reconstruction (R) and the optimization problem (LP) perform best. For the R scheme, it seems that the Van Leer limiter suits this problem better. To reach the accuracy provided by the best schemes on a moderately fine grid, one would have to use a very fine grid with the low-order scheme resulting in two orders of magnitude more runtime. This behavior is consistently reproduced for the different meshes for this test case.

### 6.3 Transport in 3D

In 3D, we test a standard first-order and the three reconstruction approaches on two different grids—tetrahedral and hexagonal prisms grids. Both grids are part of the *3D Benchmark on Discretization Schemes for Anisotropic Diffusion Problems on General Grids* presented in [11]. The coarsest version of these grids is depicted in Fig. 7. The solid body rotation test is not suitable for the considered 3D meshes since the coarse resolution does not allow to resolve the structures correctly. All the simulations are performed on a unit cube that is initially empty. A tracer enters the cube trough the side $x = 0$ with the velocity $v = (1, 0, 0)^T$. The simulation stops at the final time $T_{\text{final}} = 0.5$.

In Fig. 8 (top), we present the convergence of the different schemes and the CPU times for the 3D transport test case on tetrahedral grids. All schemes behave as expected except for the optimization-based reconstruction which failed to converge for the finer tetrahedral grids. This might be due to need of picking suitable start conditions for the linear programming. For the other schemes, the behavior is similar as for the transport problem in 2D on triangular meshes. This is not the case for the results on polyhedral meshes which are presented in the lower part of Fig. 8. We discover that, due to the large number of neighbors a grid cell can have, the least squares approach (LS) does not yield a higher-order scheme on these meshes. The selected reconstruction (R) and the optimization-based reconstruction (LP) are able to provide a higher-order alternative in this case. Again, LP and the R scheme with Minmod limiter produce similar results. The best scheme in this case is the R scheme with the van Leer limiter in both accuracy and run time to accuracy followed by the LP scheme. The first-order scheme cannot match the resolution of the second-order schemes on the coarsest grids when running on the finest grid. This means that for these more complicated grids the truly second schemes clearly outperform the low-order schemes by orders of magnitude.

### 6.4 Buckley-Leverett in 3D

In this section, we repeat the test case from Section 6.2 on the series of tetrahedral and polyhedral meshes representing the three-dimensional unit cube.

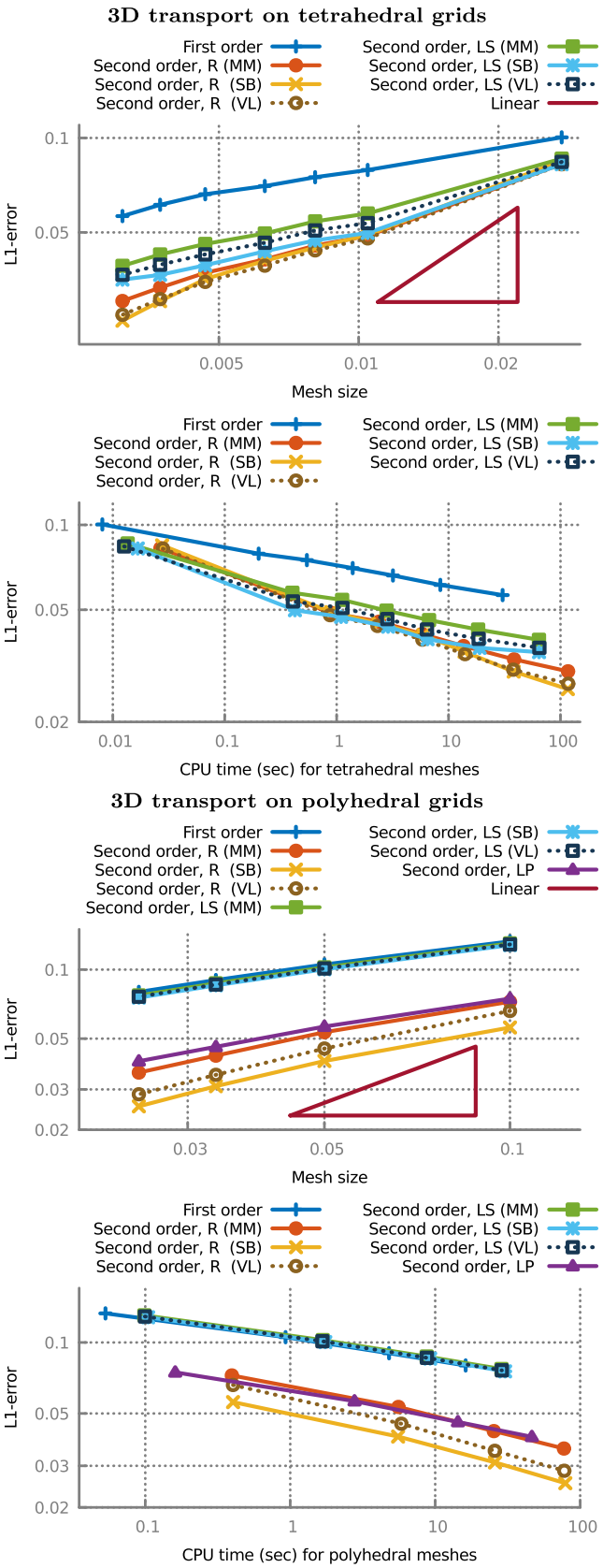


**Fig. 8** Convergence and CPU times for the 3D transport test case on a series of tetrahedral (*top*) and polyhedral (*bottom*) grids at $T_{\text{final}} = 0.5$

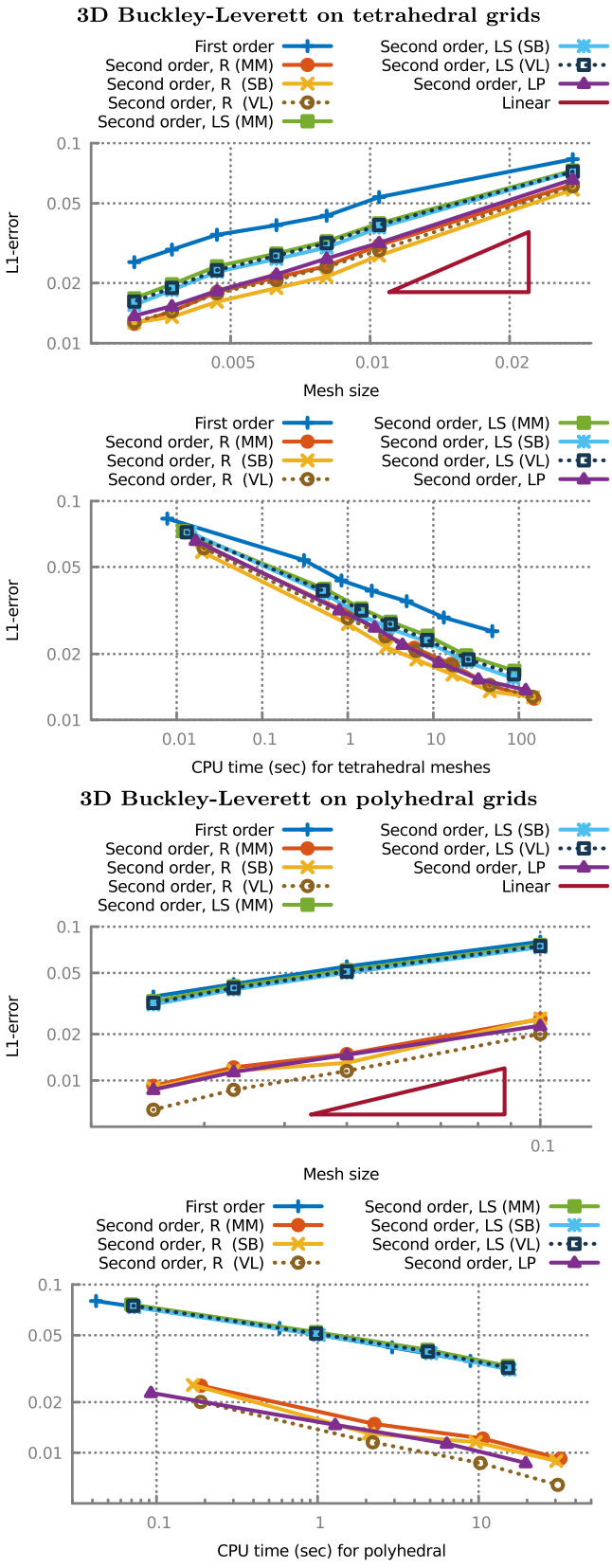


**Fig. 9** Convergence and CPU times for the 3D Buckley-Leverett test case on a series of tetrahedral (*top*) and polyhedral (*bottom*) grids at $T_{\text{final}} = 0.45$

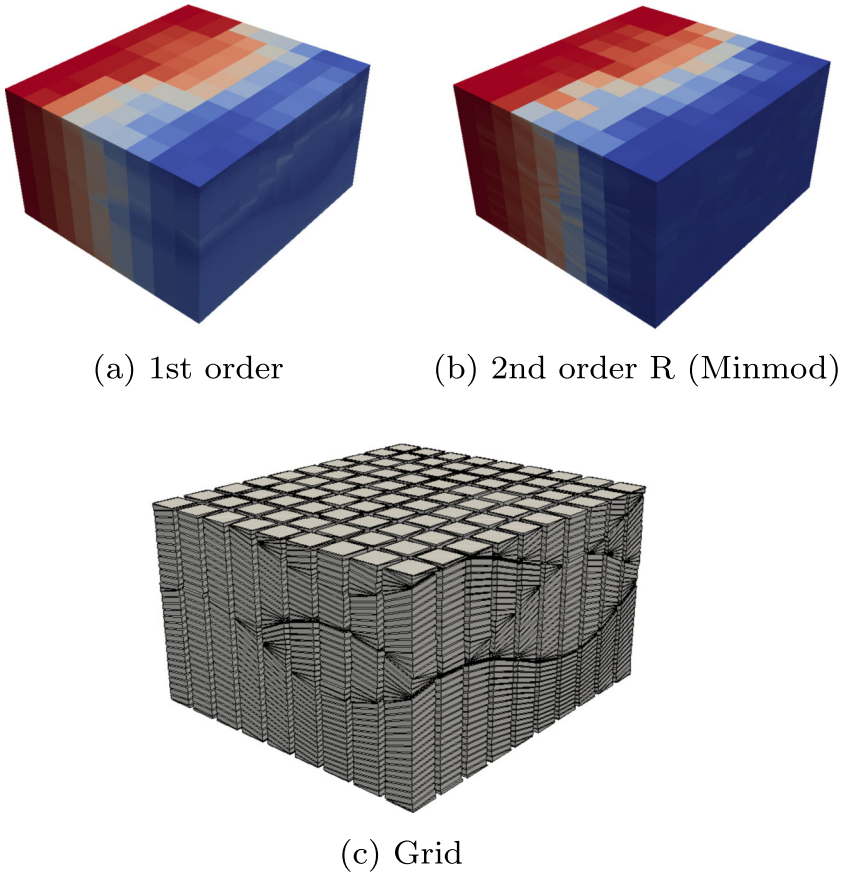


**Fig. 10** Comparison of the first- and second-order R (*Minmod*) scheme for a realistic reservoir geometry

In Fig. 9 (top), we present the convergence of the different schemes and the CPU times. The selected reconstruction scheme (R) and the optimization scheme (LP) provide the best mesh size to error ratio. In terms of performance, these schemes also provide the best accuracy for CPU time ratio. As expected, the LP scheme coincides with the selected reconstruction using a Minmod limiter function. Using the van Leer or Superbee limiter, the selected reconstruction yields slightly better results. Overall, the second-order schemes provide an excellent alternative compared to the standard first-order scheme. For example, to achieve an error of 0.3, the selected reconstruction scheme uses about 1 s of CPU time, whereas the first-order scheme can only provide this on five-times finer grid using a CPU time of around 50 s. When compared on the same grid, the least squares approach is about twice more expensive compared to the first-order scheme, whereas the selected reconstruction is about three times more expensive keeping in mind that the resulting error is much better.

In Fig. 9 (bottom), we present the convergence of the different schemes and the CPU times for the Buckley-Leverett test case on polyhedral grids. As for the 3D transport case, we see that the least squares approach (LS) does not yield a higher-order scheme on these meshes due to the many constraints the cell can have (many neighboring cells) and, thus, results in a first-order scheme. The selected reconstruction (R) and the optimization problem (LP) are again able to provide a higher-order alternative in this case. Again, LP and the R scheme with Minmod limiter produce similar results. The best scheme in this case is the R scheme with the van Leer limiter in both accuracy and run time to accuracy followed by the LP scheme. The first-order scheme run on the finest mesh cannot match the resolution of the second-order schemes when run on the coarsest grid. This means that for these more complicated grids the truly second schemes clearly outperform the low-order schemes by orders of magnitude.

### 6.5 Reservoir grids

We use the tracer test from the previous section to show the effectiveness of the proposed reconstructions on more complicated reservoir geometries. The tracer enters trough the side $x = 0$ with the velocity $v = (1, 0, 0)^T$. Since the geometry is smaller, the simulation stops at the final time $T_{\text{final}} = 0.05$. In Fig. 10, the results for the first- and the second-order R scheme are presented. Both schemes shows good performance on this more complicated geological representation. However, there is a clear advantage of the higher-order scheme on this grid.

## 7 Conclusions and future work

We presented a reconstruction based approach for second-order finite volume schemes on polygonal and polyhedral meshes. A comparison between a simple least squares approach, a more sophisticated selective reconstruction approach, and an optimization-based reconstruction technique has been carried out on 2D Cartesian, triangular and polygonal meshes as well as 3D tetrahedral meshes and prism meshes with hexagonal basis. While all second-order schemes show consistently better results on triangular meshes, the potentially large number of neighbors of polygonal and polyhedral meshes adds to the complexity of the problem.

The simplicity of the least squares approach leads to an efficient reconstruction, but tends to overeager limitation. The selective reconstruction, on the other hand, provides better accuracy at the expense of around 50% more CPU time consumption over the least squares approach. The reconstruction based on linear programming provides a good compromise between the two approaches in terms of complexity and accuracy. It is, however, limited to Minmod-type reconstructions and the selective reconstruction scheme yields better accuracy when used with a van Leer or Superbee limiter.

The presented results also show that both the selective reconstruction scheme and the LP reconstruction work on grids typically used in reservoir simulation.

Future work will focus on further improvement of the selective reconstruction scheme to for avoidance of the super linear dependence on the number of neighbors. In addition, we will focus on the integration of the second-order schemes in the open-source framework Open Porous Media (OPM).

**Acknowledgements** Robert Klöfkorn and Anna Kvashchuk thank the Research Council of Norway and the industry partners—ConocoPhillips Skandinavia AS, BP Norge AS, Det Norske Oljeselskap AS, Eni Norge AS, Maersk Oil Norway AS, DONG Energy AS Denmark, Statoil Petroleum AS, ENGIE E&P NORGE AS, Lundin Norway AS, Halliburton AS, Schlumberger Norge AS, Wintershall and Norge AS—of The National IOR Centre of Norway for the financial support.

## References

1. Aziz, K.: Reservoir simulation grids: opportunities and problems. J. Petrol. Technol. **45** (1993). doi:10.2118/25233-PA
2. Bastian, P., Blatt, M., Dedner, A., Engwer, C., Klöfkorn, R., Kornhuber, R., Ohlberger, M., Sander, O.: A generic grid interface for parallel and adaptive scientific computing. Part II: implementation and tests in DUNE. Computing **82**(2–3), 121–138 (2008). doi:10.1007/s00607-008-0004-9
3. Bastian, P., Blatt, M., Dedner, A., Engwer, C., Klöfkorn, R., Ohlberger, M., Sander, O.: A generic grid interface for parallel and adaptive scientific computing. Part I: abstract framework. Computing **82**(2–3), 103–119 (2008). doi:10.1007/s00607-008-0003-x
4. Blatt, M., Burchardt, A., Dedner, A., Engwer, C., Fahlke, J., Flemisch, B., Gersbacher, C., Gräser, C., Gruber, F., Grüninger, C., Kempf, D., Klöfkorn, R., Malkmus, T., Müthing, S., Nolte, M., Piatkowski, M., Sander, O.: The distributed and unified numerics environment, version 2.4. Arch. Numer. Softw. **4**(100), 13–29 (2016). doi:10.11588/ans.2016.100.26526
5. Buffard, T., Clain, S.: Monoslope and multislope MUSCL methods for unstructured meshes. J. Comput. Phys. **229**(10), 3745–3776 (2010). doi:10.1016/j.jcp.2010.01.026
6. Calgaro, C., Chane-Kane, E., Creuse, E., Goudon, T.: $L^\infty$-stability of vertex-based MUSCL finite volume schemes on unstructured grids: simulation of incompressible flows with high density ratios. J. Comput. Phys. **229**(17), 6027–6046 (2010). doi:10.1016/j.jcp.2010.04.034
7. Chen, L., Li, R.: An integrated linear reconstruction for finite volume scheme on unstructured grids. J. Sci. Comput. **68**(3), 1172–1197 (2016). doi:10.1007/s10915-016-0173-1
8. Dedner, A., Klöfkorn, R.: A generic stabilization approach for higher order discontinuous Galerkin methods for convection dominated problems. J. Sci. Comput. **47**(3), 365–388 (2011). doi:10.1007/s10915-010-9448-0
9. Dedner, A., Klöfkorn, R., Nolte, M., Ohlberger, M.: A generic interface for parallel and adaptive scientific computing: abstraction principles and the DUNE-Fem module. Computing **90**(3–4), 165–196 (2010). doi:10.1007/s00607-010-0110-3
10. Durlofsky, L., Engquist, B., Osher, S.: Triangle based adaptive stencils for the solution of hyperbolic conservation laws. J. Comput. Phys. **98**(1), 64–73 (1992)
11. Eymard, R., Henry, G., Herbin, R., Hubert, F., Klöfkorn, R., Manzini, G.: 3D benchmark on discretization schemes for anisotropic diffusion problems on general grids. In: Fort, J., Fürst, J., Halama, J., Herbin, R., Hubert, F. (eds.) Finite Volumes for Complex Applications VI Problems & Perspectives, Springer Proceedings in Mathematics, vol. 4, pp. 895–930. Springer, Berlin Heidelberg (2011). doi:10.1007/978-3-642-20671-9_89
12. Feistauer, M., Felcman, J., Straskraba, I.: Mathematical and Computational Methods for Compressible Flow. Oxford University Press (2003)
13. Heinemann, Z., Brand, C., Munka, M., Chen, Y.: Modeling Reservoir Geometry With Irregular Grids. SPE Res. Eval. Eng. 225–232 (1991). doi:10.2118/18412-PA
14. Herbin, R., Hubert, F.: Benchmark on discretization schemes for anisotropic diffusion problems on general grids. In: Finite Volumes for Complex Applications V, pp. 659–692. ISTE, London (2008)
15. Hou, J., Liang, Q., Zhang, H., Hinkelmann, R.: An efficient unstructured MUSCL scheme for solving the 2D shallow water equations. Environ. Modell. Softw. **66**, 131–152 (2015). doi:10.1016/j.envsoft.2014.12.007
16. Hubbard, M.: Multidimensional slope limiters for MUSCL-type finite volume schemes on unstructured grids. J. Comput. Phys. **155**(1), 54–74 (1999). doi:10.1006/jcph.1999.6329
17. Ju, L., Ringler, T., Gunzburger, M.: Numerical Techniques for Global Atmospheric Models. chap. Voronoi Tessellations and Their Application to Climate and Global Modeling, pp. 313–342. Springer Berlin Heidelberg, Berlin Heidelberg (2011)
18. Kiris, C.C., Housman, J.A., Barad, M.F., Sozer, E., Brehm, C., Moini-Yekta, S.: Computational framework for launch, ascent, and vehicle aerodynamics (LAVA). Aerospace Science and Technology, pp– (2016). doi:10.1016/j.ast.2016.05.008

19. Klöfkorn, R., Kröner, D., Ohlberger, M.: Local adaptive methods for convection dominated problems. Int. J. Numer. Methods Fluids **40**(1-2), 79–91 (2002). doi:10.1002/fld.268
20. Knoll, D.A., Keyes, D.E.: Jacobian-free Newton-Krylov methods: a survey of approaches and applications. J. Comput. Phys. **193**(2), 357–397 (2004). doi:10.1016/j.jcp.2003.08.010
21. Kröner, D.: Numerical Schemes for Conservation Laws. Wiley-Teubner (1997)
22. Lamine, S., Edwards, M.: Multidimensional upwind schemes and higher resolution methods for three-component two-phase systems including gravity driven flow in porous media on unstructured grids. Comput. Methods Appl. Mech. Eng. **292**, 171–194 (2015). doi:10.1016/j.cma.2014.12.022
23. van Leer, B.: Towards the ultimate conservative difference scheme. II. Monotonicity and conservation combined in a second-order scheme. J. Comput. Phys. **14**(4), 361–370 (1974). doi:10.1016/0021-9991(74)90019-9
24. LeVeque, R.: Numerical Methods for Conservation Laws. Birkhäuser, Basel (1990)
25. LeVeque, R.: High-resolution conservative algorithms for advection in incompressible flow. SIAM J. Numer. Anal. **33**(2), 627–665 (1996). doi:10.1137/0733033
26. May, S., Berger, M.: Two-dimensional slope limiters for finite volume schemes on non-coordinate-aligned meshes. SIAM J. Sci. Comput. **35**(5), A2163—A2187 (2013). 10.1137/120875624
27. Møyner, O., Lie, K.A.: A multiscale restriction-smoothed basis method for high contrast porous media represented on unstructured grids. J. Comput. Phys. **304**, 46–71 (2016). doi:10.1016/j.jcp.2015.10.010
28. Shu, C.-W.: High order WENO and DG methods for time-dependent convection-dominated PDEs: A brief survey of several recent developments. J. Comput. Phys. **316**, 598–613 (2016). doi:10.1016/j.jcp.2016.04.030
29. Toro, E. Riemann Solvers and Numerical Methods for Fluid Dynamics. A Practical Introduction, 2nd edn. Springer, Berlin (1999)
30. Wesenberg, M.: Efficient finite – volume schemes for magneto-hydrodynamics simulations in solar physics. Ph.D. thesis. Albert–Ludwigs–Universität Freiburg, Mathematisches Institut (2003). http://www.freidok.uni-freiburg.de/volltexte/792/